



# Modeling elongational viscosity and brittle fracture of polystyrene solutions

Manfred H. Wagner<sup>1</sup> · Esmail Narimissa<sup>2,3</sup> · Leslie Poh<sup>2,3</sup> · Taisir Shahid<sup>4,5</sup>

Received: 14 February 2021 / Revised: 13 April 2021 / Accepted: 29 April 2021 / Published online: 14 June 2021  
© The Author(s) 2021

## Abstract

Elongational viscosity data of well-characterized solutions of 3–50% weight fraction of monodisperse polystyrene PS-820k (molar mass of 820,000 g/mol) dissolved in oligomeric styrene OS8.8 (molar mass of 8800 g/mol) as reported by André et al. (Macromolecules 54:2797–2810, 2021) are analyzed by the Extended Interchain Pressure (EIP) model including the effects of finite chain extensibility. Excellent agreement between experimental data and model predictions is obtained, based exclusively on the linear-viscoelastic characterization of the polymer solutions. The data were obtained by a filament stretching rheometer, and at high strain rates and lower polymer concentrations, the stretched filaments fail by rupture before reaching the steady-state elongational viscosity. Filament rupture is predicted by a criterion for brittle fracture of entangled polymer liquids, which assumes that fracture is caused by scission of primary C–C bonds of polymer chains when the strain energy reaches the bond-dissociation energy of the covalent bond (Wagner et al., J. Rheology 65:311–324, 2021).

**Keywords** Polymer melt · Polymer solution · Fracture · Failure · Chain scission · Elongation · EIP model · Interchain pressure · Finite extensibility

## Introduction

Substantial progress in measuring the elongational viscosity of polymer melts and solutions up to high Hencky strains was made by the use of the filament stretching rheometer with locally controlled deformation and deformation rate

developed by Hassager and coworkers (Huang et al. 2016a). By measuring the local diameter of the polymer sample during elongation, the true Hencky strain and strain rate can be determined and controlled, while by elongational rheometers prescribing the global deformation of the filament only nominal values of strain and strain rate can be obtained. Elongational viscosity measurements with filament stretching rheometers have revealed surprising differences between the elongational rheology of polymer melts and solutions (Huang et al. 2013a, 2013b), which in turn has sparked different theoretical explanations as discussed, e.g., in Narimissa et al. (2020a, 2021) and Ianniruberto et al. (2020).

Progress in understanding failure of polymer samples in elongational flow was hampered by the fact that failure of stretched filaments includes the phenomena of ductile failure (“necking”) and cohesive failure (“rupture” or “brittle fracture”), and until recently, the experimental separation of these two fundamentally different failure modes has been difficult or even impossible. A further achievement of the filament stretching rheometer as shown by Huang et al. (2016b), Huang and Hassager (2017) and Huang (2019) was that when the true Hencky strain rate is controlled rather than nominal Hencky rate, the four failure zones of the so-called Malkin plot (Malkin and Petrie 1997) (purely viscous zone,

✉ Manfred H. Wagner  
manfred.wagner@tu-berlin.de

✉ Esmail Narimissa  
esmaeiln@technion.ac.il

<sup>1</sup> Polymer Engineering/Polymer Physics, Berlin Institute of Technology (TU Berlin), Ernst-Reuter-Platz 1, 10587 Berlin, Germany

<sup>2</sup> Department of Chemical Engineering, Technion–Israel Institute of Technology (IIT), Technion City, 32 000 Haifa, Israel

<sup>3</sup> Department of Chemical Engineering, Guangdong Technion–Israel Institute of Technology (GTIIT), Shantou 515063, China

<sup>4</sup> Bio and Soft Matter, Institute on Condensed Matter and Nano-science, Université catholique de Louvain, Louvain-la-Neuve, Belgium

<sup>5</sup> DSM Materials Science Center, P.O. Box 18, NL-6160 MD Geleen, The Netherlands

viscoelastic zone with failure by necking, rubbery zone, glassy zone) are reduced to just two possible states: liquid or solid, and a clear distinction exists between liquid-like behavior (unlimited steady-state elongation) and solid-like behavior (brittle fracture). A quantitative criterion for brittle fracture of entangled polymer liquids (Wagner et al. 2018) was recently extended by taking finite chain extensibility and polymer fraction of the solutions into account (Wagner et al. 2021). Filament rupture follows from scission of primary C-C bonds, when the strain energy of an entanglement segment reaches the bond-dissociation energy of the covalent bond. Thermal fluctuations lead to short-time concentration of the strain energy on one C-C bond of the entanglement segment, and the chain ruptures.

In the present paper, we analyze the elongational viscosity data of well-characterized solutions of 3–50% mass fraction of monodisperse polystyrene (PS-820k with a molar mass of 820,000 g/mol) dissolved in oligomeric styrene (OS8.8 with a molar mass of 8800 g/mol) as reported by Shahid (2018) and André et al. (2021). The polymer solutions show increasing strain hardening behavior with decreasing polymer concentration, which is associated with an increasing tendency of filament rupture at higher elongation rates. Experimental data of elongational stress growth coefficient and steady-state elongational viscosity as well as stress and strain at fracture are compared to the prediction of the Extended Interchain Pressure (EIP) model (Narimissa et al. 2020a, 2021) including the effects of finite chain extensibility and a recently developed fracture criterion for brittle fracture of polymer melts and solutions (Wagner et al. 2021). Modeling is based exclusively on linear-viscoelastic characterization of the solutions and the ratio of carbon-carbon bond energy to thermal energy, and does not require any fit parameter. The EIP model with the fracture criterion is the only model presently available for quantitative modeling of time-dependent nonlinear-viscoelastic flows including brittle fracture of polymer systems.

The paper is organized as follows: We first give a short report of the experimental data and the linear-viscoelastic characterization of the polymer systems considered, followed by a short account of the EIP model and the fracture criterion. The main focus of the paper is on comparison of experimental data and model predictions, and on the conclusions that can be drawn from this comparison.

## Experimental data and linear-viscoelastic characterization

The polymer PS-820k with a molar mass of 820 kg/mol and polydispersity index of 1.02 was obtained from Polymer Source, Inc. (Montreal, Canada). Preparation of solutions is described in detail by Shahid (2018) and André et al. (2021), and the molecular characteristics of the polystyrene solutions are summarized in Table 1. The samples are named in the

form of PS-820k/8.8k-X, where 820k characterizes the molar mass of the polystyrene, 8.8k the molar mass of the oligomeric styrene solvent with 8.8 kg/mol and with polydispersity index of 1.1, and X the percentage of mass and (assuming equal density of PS melt and solution) volume fraction of the PS in the solution.

Details of mechanical spectroscopy and elongational viscosity measurements are presented in Shahid (2018). Elongational measurements using a VADER 1000 (Huang et al. 2016a) were performed at  $T = 130$  °C. Storage ( $G'$ ) and loss modulus ( $G''$ ) were measured at iso- $T_g$  temperatures  $T_0$ , i.e., temperatures with equal distance to the glass transition temperature  $T_g$  with  $T_0 = T_g + 23.4$  K, and shifted to  $T = 130$  °C by time-temperature shifting (TTS) according to the WLF equation with shift factor  $a_{T_g}$

$$\log_{10} a_{T_g} = \frac{-c_1^0(T-T_0)}{c_2^0(T-T_0)} \quad (1)$$

and coefficients  $c_1^0 = 8.99$  and  $c_2^0 = 81.53$  K (Wagner 2014). From the mastercurves of  $G'$  and  $G''$ , parsimonious relaxation spectra were obtained,

$$G(t) = \sum_i g_i \exp(-t/\tau_i) \quad (2)$$

for characterization of the linear viscoelasticity (LVE) in the experimentally accessible window of all polymer systems considered here. The partial moduli  $g_i$  and relaxation times  $\tau_i$  as determined by the IRIS software (Winter and Mours 2006) result in excellent agreement with the linear-viscoelastic data of  $G'$  and  $G''$  (see Fig. S1 and Table S1 of the Support Information).

From the plateau modulus  $G_N$

$$G_N = \frac{\rho RT}{M_e} \quad (3)$$

the entanglement molar mass  $M_e$  is obtained, and with  $M$  being the molar mass of the polymer, the number of entanglements per chain  $Z$  is given by

$$Z = \frac{M}{M_e} \quad (4)$$

The relation between the entanglement molar mass of the polymer in solution,  $M_e$ , and entanglement molar mass in the melt,  $M_{em}$ , is given by

$$M_e = M_{em} \varphi^{-\alpha} \quad (5)$$

with  $\varphi$  being the polymer volume fraction in the solution. To be consistent with earlier works (Huang et al. 2013a, 2013b, 2016b; Wagner 2014; Narimissa et al. 2020a, 2021), we take  $G_N = 2.5 \cdot 10^5$  Pa and  $M_{em} = 13,300$  g/mol for polystyrene in the melt state. (The index  $m$  characterizes the melt state in the

**Table 1** Sample characterization at T = 130 °C

	PS-820k melt	PS-820k/8.8k-50	PS-820k/8.8k-40	PS-820k/8.8k-30	PS-820k/8.8k-20	PS-820k/8.8k-10	PS-820k/8.8k-05	PS-820k/8.8k-03
$T_g$ [°C]	106.6	102.3	101.3	100.7	99.8	98.6	98.4	98.1
$a_{T_g}$ [-]	1	0.35	0.28	0.25	0.20	0.16	0.15	0.14
$M_e$ [kg/mol]	13.3	26.6	33.3	44.3	66.5	133	266	443
$Z$ [-]	61.7	30.8	24.7	18.5	12.3	6.2	3.1	1.8
$N_e$	21.8	43.6	54.5	72.7	109	218	436	727
$\eta_0$ [Pa s]	1.07E+10	3.87E+8	1.46E+8	4.01E+7	8.01E+6	6.01E+5	1.02E+5	3.01E+4
$\tau_d$ [s]	429,918	21,461	12,634	6631	4369	1591	906	114
$\tau_R$ [s]	1644	628	505	369	293	259	248	233

following.) The value of the dilution exponent  $\alpha$  is model dependent ( $1 < \alpha < 4/3$ ), and a value of  $\alpha = 1$  is taken here. The number of Kuhn segments or “monomers” between entanglements is  $N_e = M_e/M_0$ , where  $M_0 = 610$  g/mol is the molar mass of the Kuhn monomer assumed to be independent of dilution.

According to the Doi-Edwards model, the Rouse time  $\tau_R$ , the disengagement (or reptation) time  $\tau_d$ , and the zero-shear viscosity  $\eta_0$  are given by (Dealy et al. 2018)

$$\tau_R = Z^2 \tau_e \tag{6}$$

$$\tau_d = 3Z\tau_R \tag{7}$$

$$\eta_0 = \frac{\pi^2}{12} G_N \tau_d \tag{8}$$

$\tau_e$  is the entanglement segment equilibration time. We identify here  $\tau_d$  with the mean quadratic average of the relaxation times of the discrete relaxation spectrum and calculate  $\eta_0$  from the discrete relaxation spectrum:

$$\tau_d = \frac{\sum_i g_i \tau_i^2}{\sum_i g_i \tau_i} \tag{9}$$

$$\eta_0 = \sum_i g_i \tau_i \tag{10}$$

We use Osaki’s approach (Osaki et al. 1982; Takahashi et al. 1993; Isaki et al. 2003; Menezes and Graessley 1982) for the quantification of the Rouse time  $\tau_R$ , which extrapolates the Rouse time of unentangled polymer systems to the Rouse time of entangled polymer melts and solutions, and takes into account the power of 3.4 scaling of the zero-shear viscosity with molar mass  $M$  and polymer fraction  $\varphi$  (Wagner 2014). This leads to the relation

$$\tau_R = \frac{12M\eta_0}{\pi^2 \rho RT \varphi} \left( \frac{M_{cm}}{M\varphi} \right)^{2.4} \tag{11}$$

for the Rouse stretch relaxation time.  $M_{cm}$  denotes the critical molar mass in the melt state, when the entanglement effect becomes apparent by a change of the power of 1 to power of 3.4 scaling of the zero-shear viscosity as a function of molar mass. For monodisperse polystyrene, we take the well-documented value of  $M_{cm} = 35$  kg/mol (Wagner 2014), and Eq. (11) has been used successfully for the modeling of the transient and steady-state elongational and shear viscosities of PS melts and well-entangled polymer solutions (Narimissa et al. 2020a, 2020b, 2021; Wagner et al. 2021).

For the solutions of PS-820k in OS8.8k, the power of 3.4 scaling of the zero-shear viscosity of polymer solutions with polymer fraction  $\varphi$  at iso- $T_g$  temperatures of  $T_0 = T_g + 23.4$  K is shown in Fig. 1. The solutions with polymer fractions of 50, 40, 30, and 20% (full symbols in Fig. 1) follow nicely the relation  $\eta_0 = \eta_{0m} \varphi^{3.4}$  with a value of  $\eta_{0m} = 1.07 \cdot 10^{10}$  Pas for the zero-shear viscosity of the melt, while for solutions with polymer fractions of 5 and 3% (open symbols), the zero-shear viscosity is higher than expected, possibly affected by the viscosity of the solvent OS8.8k, which has a value of  $\eta_0 = 1.0 \cdot 10^4$  Pas at 130 °C. Thus, the solutions with polymer fractions  $\varphi \leq 0.1$  deviate from the scaling presumed by Eq. (11) and cannot be determined from this relation. To be consistent with previous investigations (Narimissa et al. 2020a; Wagner et al. 2021), we calculate  $\tau_R$  by using Eq. (11) for melt 820k and its solutions with polymer fractions of 20–50%, while at lower polymer concentration, the Rouse time of the solution is taken as the time-temperature-shifted value of the Rouse time of the melt.

Table 1 shows glass transition temperature ( $T_g$ ), shift factor ( $a_{T_g}$ ), entanglement molar mass ( $M_e$ ), number of entanglements per chain ( $Z$ ), number of Kuhn monomers ( $N_e$ ) per entanglement, zero-shear viscosity ( $\eta_0$ ), disengagement/reptation time ( $\tau_d$ ), and Rouse stretch relaxation time ( $\tau_R$ ) at T = 130 °C of the monodisperse polymer samples considered in this study.

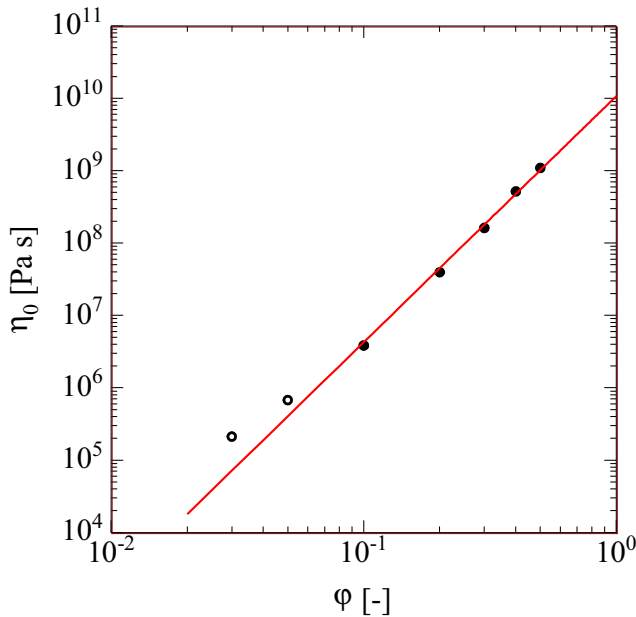


**Fig. 1** Zero-shear viscosity of solutions of PS-820k in OS8.8 with polymer fractions of 50, 40, 30, and 20% (full symbols), and 5 and 3% (open symbols) at iso- $T_g$  temperatures  $T_0 = T_g + 23.4$  K. Line indicates the relation of  $\eta_0 = \eta_{0m}\varphi^{3.4}$  with  $\eta_{0m} = 1.07 \cdot 10^{10}$  Pas

**The Extended Interchain Pressure (EIP) model**

The molecular stress function (MSF) model is a generalized tube segment model with strain-dependent tube diameter (Wagner 1990; Wagner and Schaeffer 1992; Wagner et al. 2001, 2003, 2005; Narimissa et al. 2021b). The extra stress tensor  $\sigma(t)$  of the MSF model with consideration of finite chain extensibility effects (Rolon-Garrido et al. 2006) is given by a history integral of the form

$$\sigma(t) = \int_{-\infty}^t \frac{\partial G(t-t')}{\partial t'} f \lambda \mathbf{S}_{DE}^{IA}(t, t') dt' \tag{12}$$

$t$  is the time of observation when the stress is measured, and  $t'$  indicates the time when a tube segment was created by reptation. The strain measure  $\mathbf{S}_{DE}^{IA}$  represents the contribution to the extra stress tensor originating from the affine rotation of the tube segments assuming “Independent Alignment (IA)” (Doi and Edwards 1978, 1979), and is given by

$$\mathbf{S}_{DE}^{IA}(t, t') = 5 \left\langle \frac{\mathbf{u}'\mathbf{u}'}{u'^2} \right\rangle_o = 5\mathbf{S}(t, t') \tag{13}$$

with  $\mathbf{S}(t, t')$  is the relative second-order orientation tensor.  $\mathbf{u}'\mathbf{u}'$  is the dyad of a deformed unit vector  $\mathbf{u}' = \mathbf{u}'(t, t')$ ,

$$\mathbf{u}' = \mathbf{F}_t^{-1} \cdot \mathbf{u} \tag{14}$$

$\mathbf{F}_t^{-1} = \mathbf{F}_t^{-1}(t, t')$  is the relative deformation gradient tensor, and  $u'$  is the length of  $\mathbf{u}'$ . The orientation average is indicated by  $\langle \dots \rangle_o$ ,

$$\langle \dots \rangle_o \equiv \frac{1}{4\pi} \oint [\dots] \sin\theta_o d\theta_o d\phi_o \tag{15}$$

i.e., an average over an isotropic distribution of unit vectors  $\mathbf{u}$ .

$\lambda = \lambda(t, t')$  represents the inverse of the relative tube diameter  $a/a_0$ , and at the same time the relative length of a deformed tube segment,

$$\lambda(t, t') = \frac{a_0}{a(t, t')} = \frac{l(t, t')}{l_0} \tag{16}$$

At time  $t = t'$ , the tube segment was created with equilibrium tube diameter  $a_0$  and equilibrium length  $l_0$ .

In the Gaussian limit, the molecular stress function  $f$ , i.e., the relative tension in the chain, is equal to the tube stretch  $\lambda$ . However, this is valid only as long as  $\lambda < 0.5 \lambda_{max}$  (Bird et al. 1987), where  $\lambda_{max} \cong \sqrt{N_e}$  represents the maximum stretch (i.e., a fully extended chain), and  $N_e$  the number of Kuhn monomers in an entanglement segment. Outside the Gaussian regime, tension in the chain can be described by the inverse Langevin function, or, due to its mathematical complexity, approximations like the Padé approximations (Cohen 1991). Therefore, the nonlinear elasticity caused by finite extensibility (FENE) is implemented in the EIP theory in the following way:

$$f = c(\lambda)\lambda \tag{17}$$

$c$  is a nonlinear spring coefficient, representing a relative Padé inverse Langevin function with

$$c = \frac{\left(3 - \frac{\lambda^2}{\lambda_{max}^2}\right) \cdot \left(1 - \frac{1}{\lambda_{max}^2}\right)}{\left(3 - \frac{1}{\lambda_{max}^2}\right) \cdot \left(1 - \frac{\lambda^2}{\lambda_{max}^2}\right)} \tag{18}$$

Maximal stretch  $\lambda_{max}$  is defined as

$$\lambda_{max}^2 = N_e = N_{em}\varphi^{-1} \tag{19}$$

with  $N_e$  given in Table 1.

While  $\mathbf{S}_{DE}^{IA}$  is determined directly by the deformation history according to Eq. (13),  $\lambda$  is found as a solution of an evolution equation considering affine tube segment deformation balanced by Rouse relaxation and interchain pressure (Wagner et al. 2021). We modified the evolution equation of Narimissa et al. (2020a) by including the effect of finite extensibility into the interchain pressure term in the same way as explained in detail by Rolon-Garrido et al. (2006),

$$\frac{\partial \lambda}{\partial t} = \lambda(\kappa : \mathbf{S}) - \frac{\lambda - 1}{\tau_R} \left(1 - \frac{2}{3}\varphi^4\right) - \frac{2\varphi^4}{9\tau_R} \lambda^2 (\lambda f^2 - 1) \tag{20}$$

In Eq. (20), the first term on the right-hand side describes an affine deformation, the second term Rouse relaxation, and the third term represents the interchain pressure contribution. Equation (20) reduces to the evolution equation of the EIP model of Narimissa et al. (2020a) in the Gaussian limit, i.e., when  $c = 1$  and  $f = \lambda$ . Equations (12) and (20) represent the EIP model with finite chain extensibility and are solved numerically.

From Eq. (20) follows at high Weissenberg numbers  $Wi = \dot{\epsilon}\tau_R$  (with elongational strain rate  $\dot{\epsilon}$ ) and large deformations, when the equilibrium stretch is reached and  $\partial\lambda/\partial t = 0$  that the product of molecular stress  $f$  and stretch  $\lambda$  is proportional to the square root of  $Wi$  and inverse proportional to the square of the polymer fraction,

$$f\lambda = c\lambda^2 = \frac{3}{2}\varphi^{-2}\sqrt{2Wi} \tag{21}$$

In this asymptotic limit and neglecting the glass transition, the tensile stress is expected to reach a value of

$$\sigma = 5G_N f\lambda = \frac{15}{2}G_N\varphi^{-2}\sqrt{2Wi} \tag{22}$$

From Eq. (22) and considering that  $G_N = G_{Nm}\varphi^2$ , the universal relation for the high  $Wi$  tensile stress of melts and solutions of Narimissa et al. (2020a) is recovered,

$$\sigma = \frac{15}{2}G_{Nm}\sqrt{2Wi} \tag{23}$$

with  $G_{Nm}$  being the plateau modulus of the melt.

### The fracture criterion

The thermal energy  $w_{eq}$  at a temperature  $T$  of 403 K (130 °C) is

$$w_{eq} = 3kT = 1.67 \cdot 10^{-20} J \tag{24}$$

with Boltzmann’s constant  $k = 1.38 \cdot 10^{-23} J/K$ . On the other hand, the bond-dissociation energy of a single carbon-carbon bond in hydrocarbons is (Wagner et al. 2018)

$$U = \frac{348kJ}{N_A} = 5.78 \cdot 10^{-19} J \cong 35w_{eq} \tag{25}$$

with Avogadro’s number  $N_A = 6.02 \cdot 10^{23}$ . Thus, the bond energy  $U$  is about 35 times larger than the thermal energy  $w_{eq}$  at 130 °C, which is why the polymer chain will not break due to Brownian motion at equilibrium.

As explained by Wagner et al. (2021), the strain energy of a chain segment is taken as

$$w(N_{em}) = 3kTf\lambda\varphi \tag{26}$$

with  $N_{em}$  being the number of Kuhn monomers of an entanglement segment in the melt. When the strain energy of the segment reaches the critical energy

$$w_c = 3kTf_c\lambda_c\varphi = U \tag{27}$$

the total strain energy of the chain segment will be concentrated on *one* C-C bond by thermal fluctuations, and this bond then ruptures. We recall that stretch and tension are relative quantities, and therefore, the strain energy  $w = w(t, t')$  is also a relative quantity. Chain segments with long relaxation times, i.e., those preferably in the middle of the chain, will be the first to reach the critical energy  $w_c$  and will fracture. Chain segments closer to the ends of the macromolecule, which due to reptation processes have shorter relaxation times and see less stretch and tension within the time interval of  $t'$  (creation) and  $t$  (observation), will not reach  $w_c$  and are less likely to fracture. We assume that as soon as the strain energy  $w = w(t, t' = 0)$  accumulated between the start-up of deformation at time  $t' = 0$  and time  $t = t_c$  reaches the critical energy  $w_c = w(t = t_c, t' = 0)$ , a sufficient concentration of locally ruptured chains is reached and crack initiation will occur. Crack initiation is followed by crack growth, which leads within a very short time (about 200 ms according to Huang et al. (2016b)) to brittle fracture of the sample. At time  $t = t_c$ , the critical Hencky strain at fracture,  $\epsilon_c = \dot{\epsilon}t_c$ , is reached and the critical tensile stress at fracture,  $\sigma_c = \sigma(t_c)$ , is given by the stress equation (Eq. (12)). Chain fracture preferably in the middle of the polymer chain is in agreement with earlier findings of Ballauf and Wolf (1984): They studied the degradation of solutions of 4.9–20 wt% of polystyrene in trans-decalin by use of a shear cell at shear rates of  $5.0 \cdot 10^3 < \dot{\gamma} < 10^4 s^{-1}$ , and showed that only a Gaussian breakage probability of C-C bonds with the center of the probability distribution at the midpoint of the chain can reproduce the experimentally observed changes in the molar mass distribution.

From the fracture hypothesis defined by Eq. (27), the maximum achievable product of critical molecular stress  $f_c$  and critical stretch  $\lambda_c$  is obtained,

$$f_c\lambda_c\varphi = c\lambda_c^2\varphi = \frac{U}{3kT} \cong 35 \tag{28}$$

We called this fracture mode “entropic fracture” (Wagner et al. 2018), as it is caused by thermal fluctuations, in contrast to the “enthalpic fracture” hypothesis of Lake and Thomas (1967) as modified by Mazich and Samus (1990). These authors assumed that all bonds are fully stretched at fracture and when a chain with  $N$  C-C bonds between two entanglement points ruptures, the strain energy  $w_c = NU$  corresponding to the bond energy of *all*  $N$  C-C bonds in the entangled chain segment is dissipated.

Combining the fracture criterion of Eq. (28) with the asymptotic tensile stress at high  $Wi$  and large stretch according

to Eq. (22), we expect at sufficiently fast and large elongations a critical tensile stress  $\sigma_c$ ,

$$\sigma_c = 5G_N f_c \lambda_c = \frac{15}{2} G_N \varphi^{-2} \sqrt{2Wi_c} \cong 5G_N \frac{U}{3kT} \varphi^{-1} \quad (29)$$

From the first and last term of this identity, we expect the following scaling relation for the normalized critical stress  $\sigma_c \varphi / G_N$  at fracture,

$$\frac{\sigma_c \varphi}{G_N} = 5 \frac{U}{3kT} \cong 175 \quad (30)$$

The reduced critical Weissenberg number  $Wi_c / \varphi^2$  for the onset of fracture

$$\frac{Wi_c}{\varphi^2} = \frac{2}{9} \left( \frac{U}{3kT} \right)^2 \cong 272 \quad (31)$$

is obtained from the two last terms of Eq. (29).  $Wi_c$  is the minimum Weissenberg number for fracture to occur; i.e., fracture is expected only for  $Wi \geq Wi_c$ .

## Comparison of experimental data and model predictions

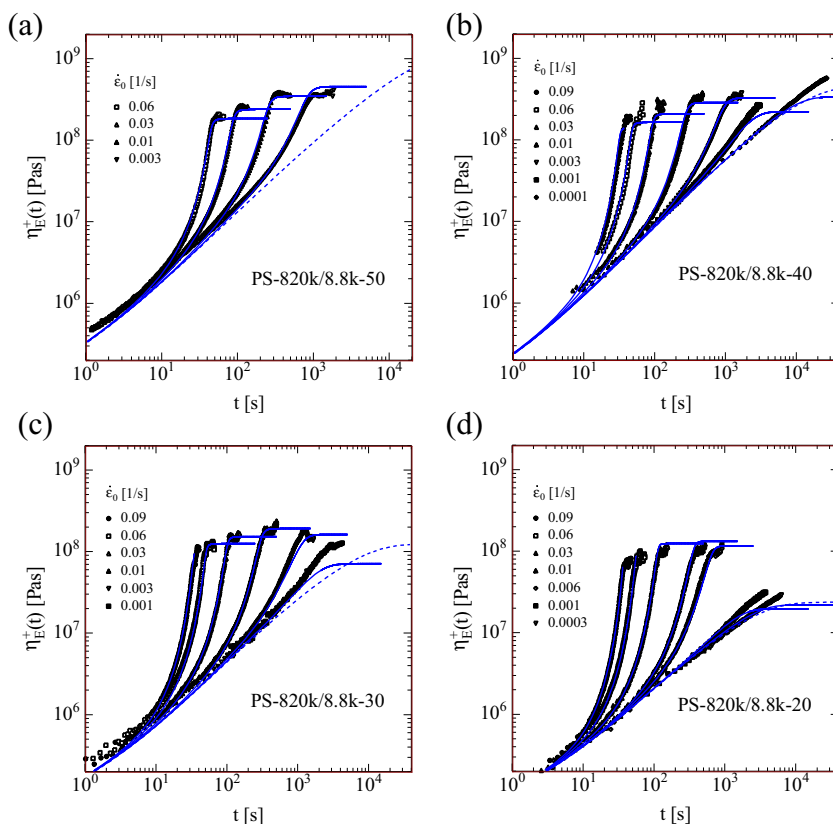
In the following, we compare predictions of the Extended Interchain Pressure (EIP) model (Eqs. (12) and (20)) and the fracture criterion (Eq. (28)) with experimental evidence. We recall that the model is based exclusively on the linear-viscoelastic characterization of the polymer solutions and the ratio of carbon-carbon bond energy to thermal energy, and does not contain any free parameter. Figure 2 presents the elongational stress growth coefficient  $\eta_E^+(t)$  as a function of time  $t$  for polymer solutions of PS-820k with polymer fractions of 50% down to 20%. Agreement of data and predictions is seen not only for the start-up of the elongational viscosity, where predictions and experimental data are nearly indistinguishable (except at low strain rates with some deviations between experiment and model), but also for the steady-state elongational viscosity, where data and predictions agree within experimental scatter. For PS-820k/8.8k-40 and PS-820k/8.8k-30, fracture is observed and predicted by the fracture criterion at the highest strain rate (0.09 s<sup>-1</sup>), and for PS-820k/8.8k-20 at the two highest strain rates (0.09 and 0.06 s<sup>-1</sup>). We note that fracture is evident in these cases by the fact that the filament fails at Hencky strains of  $\varepsilon \leq 4.2$  as shown and discussed below in Fig. 7 and that no steady-state viscosity is reached.

As demonstrated in Fig. 2, the elongational strain hardening increases with decreasing concentration of polymer PS-820k, and as discussed below, stretch and tension in the entanglement segments increase. This in turn leads to the onset

of fracture as observed experimentally and predicted by the fracture criterion at higher strain rates. For solutions with lower polymer fractions (Fig. 3), this effect becomes even more apparent: In samples with 10% polymer fraction (Fig. 3a), while at elongation rate of 0.01 s<sup>-1</sup> the indication of a steady-state elongational viscosity is noticed, filament rupture at elongation rates of 0.2 and 0.09 s<sup>-1</sup> is obvious. The elongational stress growth coefficients at elongation rates of 0.03 and 0.06 s<sup>-1</sup> show a maximum and then a drop of the viscosity, which may be interpreted as delayed fracture. Solutions with 5 and 3% polymer concentration clearly show fracture at all elongation rates investigated (Fig. 3b and c). For these solutions, there is the indication of delayed fracture due to necking; i.e., above a certain deformation, the elongational stress growth coefficient  $\eta_E^+(t)$  shows a distinctive kink to a lower slope of  $\eta_E^+(t)$  before the filament finally fails. This change of slope should not be confounded with a transition to steady-state flow, since the occurrence of steady-state flow is occurring rather abrupt as seen, e.g., in Fig. 2a. The predicted value of the viscosity at fracture coincides approximately with the position of the kink in the  $\eta_E^+(t)$  curve as seen in Fig. 3b and c. One may speculate that the high concentration of solvent OS8.8k in these solutions prevents immediate brittle fracture of the filament after breakage of polymer chains (Huang 2019). We also note that the number of entanglements in these solutions is reduced to only two or three (Table 1), and therefore, modeling based on tube segments may come to its limit. More experimental investigations will be needed to clarify this issue.

To illustrate the interactions of strain hardening, chain stretch, and fracture, Fig. 4 shows the maximal values of tension  $f$ , stretch  $\lambda$ , and reduced strain energy  $w_s = w/3kT$  as a function of the Weissenberg number  $Wi$  resulting from integration of Eq. (20) for PS-820k/8.8k-40, PS-820k/8.8k-20, and PS-820k/8.8k-05. At sufficiently small values of  $Wi$  and as long as the reduced free energy  $w_s$  is below a value of  $w_s = w/3kT = f_c \lambda_c \varphi \cong 35$ , a steady state of tension  $f$  and stretch  $\lambda$  is obtained, and consequently a steady-state elongational viscosity is predicted by the stress equation (Eq. (12)). We recall that as soon as the strain energy  $w$  accumulated since the start-up of deformation reaches the critical energy  $w_c$ , enough polymer chains will rupture and brittle fracture will occur. At this time  $t = t_c$ , the critical Hencky strain at fracture,  $\varepsilon_c = \varepsilon t_c$ , is reached and the critical tensile stress at fracture,  $\sigma_c = \sigma(t_c)$ , is given by the stress equation (Eq. (12)). Thus, when the reduced free energy reaches a value of  $w_s = w_c/3kT \cong 35$ , the polymer chain fractures and the maximal values of tension  $f = f_c$  and stretch  $\lambda = \lambda_c$  remain constant, independent of the Weissenberg number. As seen in Fig. 4a for PS-820k/8.8k-40, the critical Weissenberg number for the onset of fracture is reached at  $Wi_c = 45$  corresponding to the highest strain rate in Fig. 2b. The entanglement stretch at fracture is limited to  $\lambda = \lambda_c = 6.1$ , which means that chains at fracture are not fully

**Fig. 2** Comparison of data (symbols) and predictions (lines) of elongational stress growth coefficient  $\eta_{E}^{+}(t)$  for solutions of PS-820k in OS8.8 with polymer fractions of (a) 50, (b) 40, (c) 30, and (d) 20%. Dotted lines indicate the linear-viscoelastic elongational stress growth coefficient



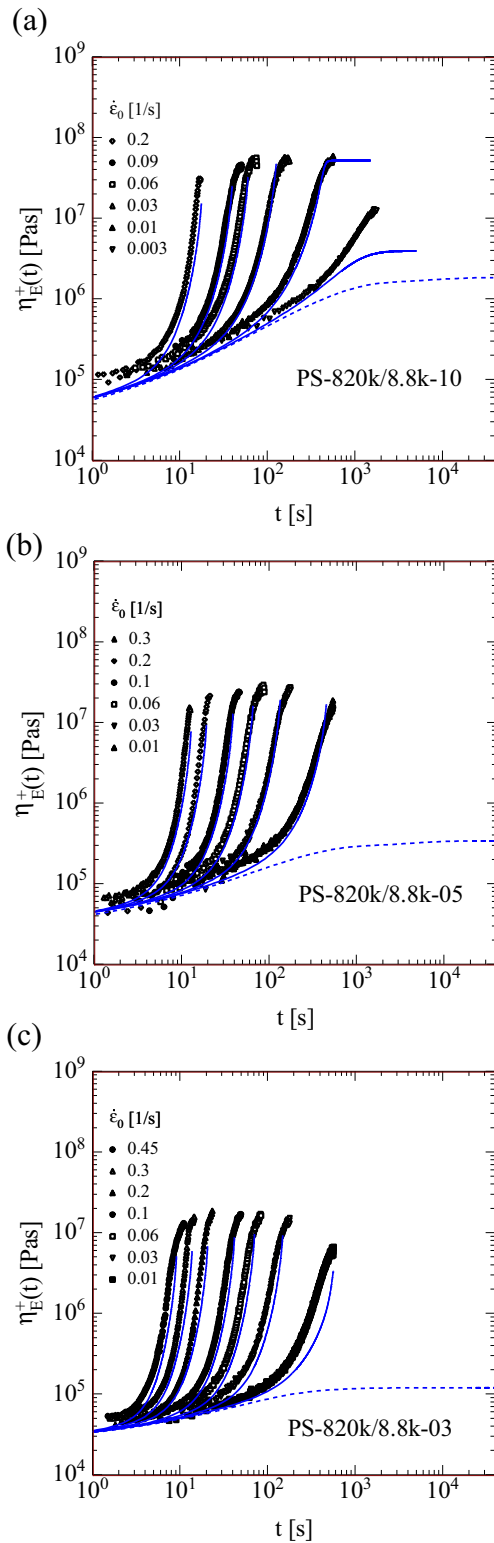
stretched, but have reached 82% of maximal stretch  $\lambda_{\max} = \sqrt{N_e} = \sqrt{54.5} = 7.4$ . The tension in the chain reaches a maximum value of  $f=f_c = 14.5$ .

With decreasing polymer fraction, the critical Weissenberg number for the onset of fracture decreases, reaching a value of  $Wi_c = 15$  for PS-820k/8.8k-20 (Fig. 4b), and the two highest strain rates shown in Fig. 2d lead to filament fracture. The stretch at fracture is limited to  $\lambda = \lambda_c = 8.6$ , which is again equivalent to 82% of maximal stretch  $\lambda_{\max} = \sqrt{N_e} = \sqrt{109} = 10.4$ , and the tension reaches a maximum value of  $f=f_c = 20.4$ . From the fracture criterion of Eq. (28) and the nonlinear spring constant  $c = c(\lambda^2, \lambda_{\max}^2)$  of Eq. (18) follows in good approximation that the ratio of chain stretch at fracture  $\lambda_c$  to maximum stretch  $\lambda_{\max} = \sqrt{N_e}$  is given by  $\lambda_c/\lambda_{\max} = 0.82$ , and the ratio of critical tension at fracture  $f_c$  to  $\lambda_c$  is  $f_c/\lambda_c = 2.4$ , independent of the polymer fraction  $\varphi$ . At a polymer fraction of  $\varphi = 0.05$ , the critical Weissenberg number for the onset of fracture is further reduced to  $Wi_c = 2$  for PS-820k/8.8k-05 (Fig. 4c). While the critical Weissenberg number for the onset of fracture is decreasing, a marked increase of maximum values of tension and stretch with decreasing polymer fraction is seen when going from  $\varphi = 0.4$  (Fig. 4a) to  $\varphi = 0.05$  (Fig. 4c), leading to a marked increase in the strain hardening of the solutions.

Also shown in Fig. 4 are predictions for the Gaussian limit, i.e., for  $\lambda_{\max}^2 = N_{em} \rightarrow \infty$ . In the Gaussian limit,  $\lambda = f = \lambda_G$

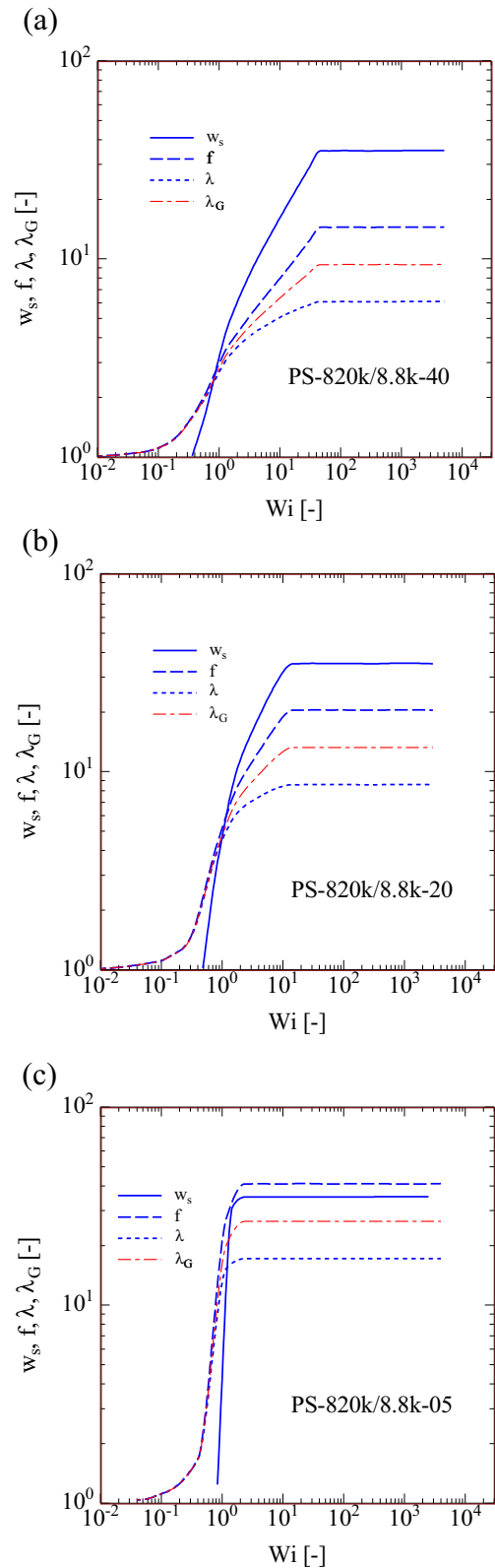
reaches a limiting value of  $\lambda_G = \lambda_c = \sqrt{\frac{U/\varphi}{3kT}} = 5.9\varphi^{-1/2}$  according to Eq. (28) with  $c = 1$ , which is larger than the maximum stretch  $\lambda_{\max} = 4.7\varphi^{-1/2}$  of the entanglement segment. This shows the importance of taking into account finite chain extensibility in the evolution equation (Eq. (20)) of the stretch.

Figure 5 presents a direct comparison of experimental data and model predictions of the steady-state elongational viscosity  $\eta_E$  at 130 °C as a function of Hencky strain rate  $\dot{\epsilon}$  for all solutions of PS-820k investigated. Full symbols and full lines indicate the measured and predicted steady-state elongational viscosity reached at sufficiently large Hencky strains, respectively, when the solutions show liquid-like behavior, i.e., unlimited deformability. Open symbols and dotted lines signify the maximal elongational viscosity at fracture and correspond to the solid-type brittle fracture behavior of the solutions. For solutions with polymer concentrations of 20–50%, fracture is observed experimentally and predicted by the model only at the highest strain rates, and fracture would be expected at even higher elongation rates as indicated by the dotted lines in Fig. 5. For solutions with lower polymer concentrations of 3–10%, fracture is observed experimentally, and also predicted by the fracture criterion, already at lower or at all strain rates investigated. The deviations seen between experimentally observed viscosities and predictions at low polymer concentrations are due to the effect of necking and delayed filament failure as mentioned earlier.



**Fig. 3** Comparison of data (symbols) and predictions (lines) of elongational stress growth coefficient  $\eta_E^+(t)$  for solutions of PS-820k in OS8.8 with polymer fractions of (a) 10, (b) 5, and (c) 3%. Dotted lines indicate the linear-viscoelastic elongational stress growth coefficient

Due to the decrease of the glass transition temperature of the polymer solutions with decreasing polymer fraction and



**Fig. 4** Normalized free energy  $w_s = w/3kT$ , tension  $f$ , and stretch  $\lambda$  of entanglement segment of solutions PS-820k/8.8k-40 (a), PS-820k/8.8k-20 (b), and PS-820k/8.8k-05 (c). Dash-dotted line is the prediction of stretch  $\lambda_G$  for the Gaussian limit ( $\lambda_{max}^2 = N_{em} \rightarrow \infty$ )



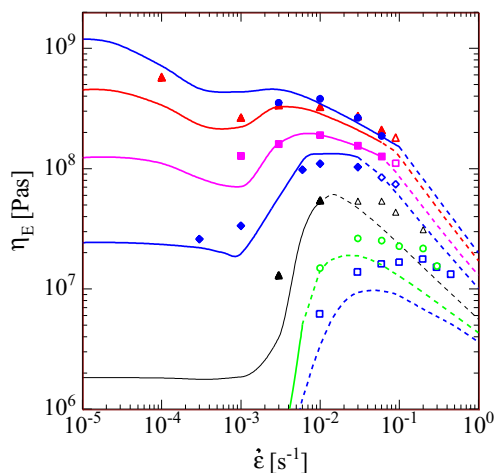
the consequential decrease of the Rouse time  $\tau_R$  at 130 °C (Table 1), the experimental window as noticed from the increasing part of the elongational viscosity in Fig. 5 is shifted to higher elongation rates at lower polymer concentrations. A comparison of the elongational viscosity  $\eta_E$  of the polymer solutions at temperatures  $T_0 = T_g + 23.4$  K with equal distance from the glass transition temperature  $T_g$  as a function of the Weissenberg number  $Wi = \dot{\epsilon}\tau_R$  is presented in Fig. 6. To account for the change in temperature, the elongational viscosity needs to be rescaled by the time-temperature shift factor  $a_{T_g}$  as given in Table 1. The long-dotted line with slope of  $-1/2$  represents the high strain and strain rate limit of the EIP model, which is obtained from Eq. (23) as

$$\eta_E = 15G_{Nm}\tau_{Rm}(2Wi)^{-1/2} \tag{32}$$

with  $G_{Nm} = 2.5 \cdot 10^5$  Pa and  $\tau_{Rm} = 1644$  s being plateau modulus and Rouse time of the melt, respectively. Relation (32), which is independent of polymer fraction  $\varphi$ , represents the upper limit of the elongational viscosity according to the EIP model assuming that no fracture occurs. At the highest strain rates measured, the experimental data of solutions PS-820k/8.8k-50 and PS-820k/8.8k-40 come closest to this line, while at lower polymer concentrations, due to early fracture the maximal elongational viscosities are much lower and do not reach this asymptotic limit.

The rescaled elongational viscosity  $\eta_E(Wi)/a_{T_g}$  shows four distinct features:

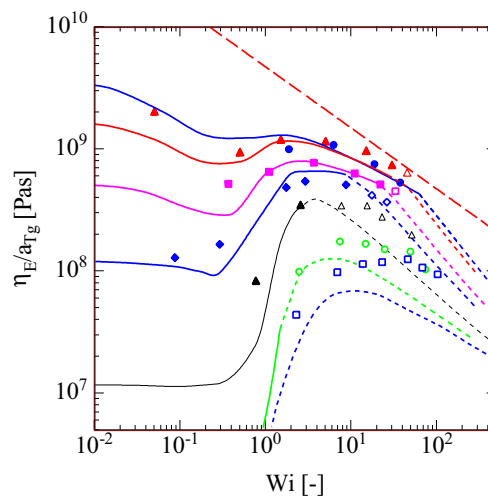
- (1). For the solutions with higher polymer fractions and at  $Wi < 1$ ,  $\eta_E$  decreases with increasing  $Wi$ . This is due to



**Fig. 5** Comparison of data (symbols) and predictions (lines) of elongational viscosity  $\eta_E$  as a function of the Hencky strain rate  $\dot{\epsilon}$  for solutions of PS-820k in OS8.8 at 130 °C. Polymer concentration from top to bottom: 50, 40, 30, 20, 10, 5, and 3%. Full symbols and full lines indicate steady state (liquid-like behavior), while open symbols and dotted lines maximum elongational viscosity at fracture (solid-like behavior)

the orientation of entanglement segments at  $\dot{\epsilon} > 1/\tau_d$  without chain stretch, and it corresponds to the prediction of the original Doi-Edwards model. At lower polymer concentration, this regime vanishes as the disentanglement time  $\tau_d$  decreases with lower polymer concentration according to  $\tau_d \propto \varphi^{1.4}$  at iso- $T_g$  temperature as shown by Wagner (2014) and approaches the Rouse time  $\tau_R$ .

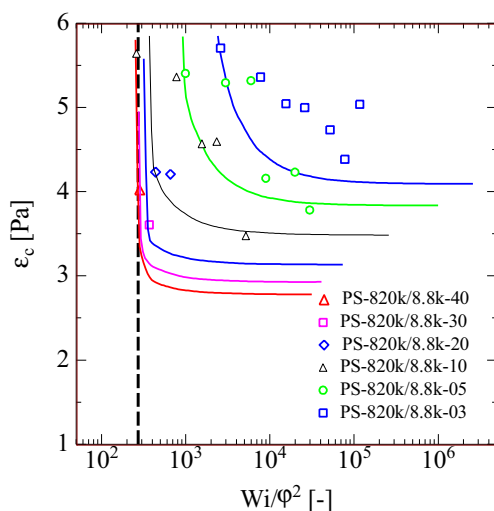
- (2). Starting at  $Wi \cong 1/3$ , an increase of  $\eta_E$  is observed which is stronger at lower polymer concentrations. In the regime of  $Wi \leq 1$ , chain stretch increases sharply due to the Rouse relaxation term in Eq. (20), until further increase is limited by the interchain pressure. The interchain pressure term is proportional to the 4th power of the polymer fraction  $\varphi$ , and thus decreases markedly with decreasing polymer concentration, which explains why lower polymer concentrations will lead to larger chain stretch and chain tension as shown in Fig. 4.
- (3). Depending on the polymer concentration, at  $Wi \geq 1$  a maximum of  $\eta_E$  is reached, and at still higher  $Wi$  the elongational viscosity decreases with a slope larger than  $-1/2$ , and approaches the universal limiting viscosity of the EIP model according to Eq. (32). The maximum followed by a decreasing regime is the signature of the interchain pressure.
- (4). At sufficiently high strain rates, the strain energy of the entanglement segment becomes so high that brittle fracture occurs and the filament breaks.



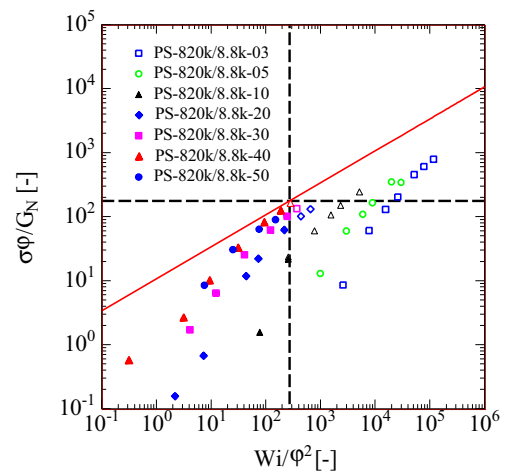
**Fig. 6** Comparison of data (symbols) and predictions (lines) of the rescaled elongational viscosity  $\eta_E/a_{T_g}$  as a function of Weissenberg number  $Wi = \dot{\epsilon}\tau_R$  for solutions of PS-820k in OS8.8 at iso- $T_g$  temperatures  $T = T_g + 23.4$  K. Polymer concentration from top to bottom: 50, 40, 30, 20, 10, 5, and 3%. Full symbols and full lines indicate steady state (liquid-like behavior), while open symbols and dotted lines maximum elongational viscosity at fracture (solid-like behavior). Long-dotted line with slope of  $-1/2$  represents high strain and strain rate limit of the EIP model (Eq. (32))

Figure 7 presents the critical strain at fracture  $\varepsilon_c$  as a function of the reduced Weissenberg number  $Wi/\varphi^2$ . The reduced critical Weissenberg number  $Wi_c/\varphi^2$  for the onset of fracture is given by Eq. (31) as  $Wi_c/\varphi^2 = 272$  and is indicated in the figure by the vertical long-dotted line. Fracture occurs only at or to the right of this line for all solutions considered. The onset of fracture of the polymer solutions of PS-820k is shifted to higher  $Wi/\varphi^2$  with decreasing polymer fraction in agreement with earlier results of other polystyrene solutions (Huang 2019; Wagner et al. 2021). The magnitude of  $\varepsilon_c$  depends on the polymer fraction  $\varphi$ , and the strain at fracture increases with decreasing polymer concentration. Predictions are in reasonable agreement with experimental data. For PS-820k/8.8k-10, PS-820k/8.8k-05, and PS-820k/8.8k-03, the experimental data points of the lowest and the highest strain rate with fracture are seen to agree quite well with predictions. For strain rates in between the lowest and the highest strain rate, the data points are shifted to the right relative to the predictions, possibly due to the necking behavior mentioned earlier, but they show the decreasing trend with increasing  $Wi$  and approach the lower level of  $\varepsilon_c$  as predicted.

The maximum values of the normalized tensile stress  $\sigma\varphi/G_N$  are presented in Fig. 8 as a function of the reduced Weissenberg number  $Wi/\varphi^2$  for all polymer solutions of PS-820k considered. The asymptotic critical reduced stress at fracture  $\sigma_c\varphi/G_N \cong 175$  at high  $Wi$  and large stretch, as expected by the scaling relation (30), is indicated by the horizontal long-dotted line. All data symbols above this line indicate fractured samples (open symbols), while below this line, there are both fractured samples (open symbols) and those which have reached steady-state stress (full symbols). The fractured samples below this line are those that did not reach the asymptotic limit before fracture. The reduced critical Weissenberg



**Fig. 7** Comparison of data (symbols) and predictions (lines) of critical Hencky strain at break  $\varepsilon_c$  as a function of reduced Weissenberg number  $Wi/\varphi^2$ . Reduced critical Weissenberg number at the onset of fracture  $Wi_c/\varphi^2 = 272$  (Eq. (31)) is indicated by vertical long-dotted line



**Fig. 8** Comparison of data (symbols) and predictions (lines) of reduced tensile stress  $\sigma\varphi/G_N$  as a function of reduced Weissenberg number  $Wi/\varphi^2$  for polymer solutions of PS-820k. Samples which have reached steady-state stress are indicated by full symbols, and fractured samples by open symbols. The asymptotic critical reduced stress at fracture of  $\sigma_c\varphi/G_N \cong 175$  (Eq. (31)) is indicated by the horizontal long-dotted line. Vertical long-dotted line represents reduced critical Weissenberg number at the onset of fracture  $Wi_c/\varphi^2 = 272$  (Eq. (30)). Full line is the high strain and strain rate limit of the melt (Eq. (23))

number  $Wi_c/\varphi^2$  for the onset of fracture given by Eq. (31) is  $Wi_c/\varphi^2 = 272$ , and it is indicated in the figure by the vertical long-dotted line. This line allows separating liquid-type and solid-type behavior: Fracture occurs only at or to the right of the vertical line for all solutions considered, while no fracture is observed to the left of this line. Steady-state stress for any polymer fraction between 3 and 100% (melt) can only be achieved in the lower left sector, below the high strain and strain rate limit given by Eq. (23) for the melt (i.e.,  $\varphi = 1$ ), indicated by the full straight line with slope of 1/2. Similar to relation (32) for the viscosity, Eq. (23) represents the upper limit of the reduced elongational stress according to the EIP model assuming that no fracture occurs. The experimental data of solutions PS-820k/8.8k-50 and PS-820k/8.8k-40 come closest to this line, while at lower polymer concentrations, the maximal elongational stresses measured are much lower due to fracture.

## Conclusions

The Extended Interchain Pressure (EIP) model (Narimissa et al. 2020a, 2021) with finite chain extensibility and a fracture criterion for brittle fracture of polymer systems (Wagner et al. 2021) allows modeling of the elongational viscosity data of a well-characterized set of monodisperse polymer solutions of PS-820k in oligomeric styrene with polymer concentrations of 3–50% (Shahid 2018; André et al. 2021), based exclusively on linear-viscoelastic characterization and the ratio of carbon-

carbon bond energy to thermal energy, and does not contain any free parameter.

The analysis substantiates and extends earlier findings of the suitability of the EIP model and the entropic fracture criterion for the modeling of the rheology and brittle fracture of monodisperse polymer melts and solutions. The essential features of the EIP model and the fracture criterion are as follows:

- Nonlinear reptation dynamics is modeled by a history integral of coupled stretch and orientation of temporary entanglement segments, thus avoiding pre-averaging of stretch and orientation (Narimissa and Wagner 2019);
- Stretch and stretch relaxation of entanglement segments are accounted for by an evolution equation of the tube diameter, which includes the effects of affine deformation, Rouse relaxation, and interchain pressure. Both Rouse relaxation and interchain pressure are governed by the Rouse time. The interchain pressure is proportional to the 4th power of the polymer fraction, and because the interchain pressure, which limits chain stretch, decreases with decreasing polymer concentration, the stretch of polymer chains increases with decreasing polymer fraction of the solutions;
- When the strain energy of a chain segment reaches the bond energy  $U$  of one carbon-carbon bond, the chain fractures and the polymer filament fails by chain scission. Chain segments with long relaxation times, i.e., those preferably in the middle of the chain, will be the first to reach the critical energy and will fracture. Chain segments closer to the ends of the chain, which due to reptation processes have shorter relaxation times and see less stretch and tension, are less likely to fracture. This is in agreement with experimental evidence of chain scission in shear degradation of polystyrene solutions (Ballauß and Wolf 1984);
- The ratio of chain stretch at fracture  $\lambda_c$  to maximum stretch  $\lambda_{\max} = \sqrt{N_e}$  is in good approximation  $\lambda_c/\lambda_{\max} = 0.82$ . Thus, the relative stretch at fracture  $\lambda_c/\lambda_{\max}$  is independent of polymer fraction; i.e., the entanglement segments of melt and solutions are stretched at fracture to the same level relative to  $\lambda_{\max}$ .
- At sufficiently large deformations and high Weissenberg numbers  $Wi$ , this results in an asymptotic critical tensile stress at fracture of  $\sigma_c = 5 \frac{U}{3kT} \frac{G_N}{\phi} \cong 175 G_{Nm} \phi$  and a critical Weissenberg number for the onset of fracture of  $Wi_c = \frac{2}{5} \left( \frac{U}{3kT} \phi \right)^2 \cong 272 \phi^2$  at 130 °C;
- The Hencky strain at fracture  $\varepsilon_c$  increases with decreasing polymer concentration  $\phi$ , and at constant  $\phi$  decreases with increasing Weissenberg number  $Wi$ .

Model predictions for elongational viscosity and fracture are in agreement with experimental evidence for all

polystyrene solutions considered. Further experiments using filament stretching rheometers with locally controlled elongational strain and strain rate will show whether the modeling concept presented here can be extended to other polymers than polystyrene (Narimissa et al. 2021) and also to bidisperse and polydisperse polymer melts and solutions.

**Supplementary Information** The online version contains supplementary material available at <https://doi.org/10.1007/s00397-021-01277-1>.

**Acknowledgements** We are grateful to Evelyne van Ruymbeke and Alexis André for technical support and helpful discussions during the preparation of this paper.

**Funding** Open Access funding enabled and organized by Projekt DEAL.

**Open Access** This article is licensed under a Creative Commons Attribution 4.0 International License, which permits use, sharing, adaptation, distribution and reproduction in any medium or format, as long as you give appropriate credit to the original author(s) and the source, provide a link to the Creative Commons licence, and indicate if changes were made. The images or other third party material in this article are included in the article's Creative Commons licence, unless indicated otherwise in a credit line to the material. If material is not included in the article's Creative Commons licence and your intended use is not permitted by statutory regulation or exceeds the permitted use, you will need to obtain permission directly from the copyright holder. To view a copy of this licence, visit <http://creativecommons.org/licenses/by/4.0/>.

## References

- André A, Shahid T, Oosterlinck F, Clasen C, van Ruymbeke E (2021) Investigating the transition between polymer melts and solutions in non-linear elongational flow. *Macromolecules* 54:2797–2810
- Ballauß M, Wolf BA (1984) Degradation of chain molecules. 2. Thermodynamically induced shear degradation of dissolved polystyrene. *Macromolecules* 17:209–216
- Bird RB, Curtiss Ch F, Armstrong RC, Hassager O (1987). Dynamics of polymeric liquids Vol. 2. *Kinetic Theory*. Wiley and Sons, USA
- Cohen A (1991) A Padé approximant to the inverse Langevin function. *Rheol Acta* 30:270–273
- Dealy JM, Read DJ, Larson RG (2018) *Structure and rheology of molten polymers: from structure to flow behavior and back again*. Carl Hanser Verlag GmbH Co KG, München
- Doi M, Edwards SF (1978) Dynamics of concentrated polymer systems. Part 3.- the constitutive equation. *J Chem Soc, Faraday Trans* 74: 1818–1832
- Doi M, Edwards SF (1979) Dynamics of concentrated polymer systems. Part 4.- rheological properties. *J Chem Soc, Faraday Trans* 75:38–54
- Huang Q, Mednova O, Rasmussen HK, Alvarez NJ, Skov AL, Almdal K, Hassager O (2013a) Concentrated polymer solutions are different from melts: role of entanglement molecular weight. *Macromolecules* 46:5026–5035
- Huang Q, Alvarez NJ, Matsumiya Y, Rasmussen HK, Watanabe H, Hassager O (2013b) Extensional rheology of entangled polystyrene solutions suggests importance of nematic interactions. *ACS Macro Lett* 2:741–744
- Huang Q, Mangnus M, Alvarez NJ, Koopmans R, Hassager O (2016a) A new look at extensional rheology of low-density polyethylene. *Rheol Acta* 55:343–350

- Huang Q, Alvarez NJ, Shabbir A, Hassager O (2016b) Multiple cracks propagate simultaneously in polymer liquids in tension. *Phys Rev Lett* 117:087801
- Huang Q, Hassager O (2017) Polymer liquids fracture like solids. *Soft Matter* 13:3470–3474
- Huang Q (2019) Exploring the mechanism of fracture for entangled polymer liquids in extensional flow. *Phys Fluids* 31:083105
- Ianniruberto G, Marrucci G, Masubuchi Y (2020) Melts of linear polymers in fast flows. *Macromolecules* 53:5023–5033
- Isaki T, Takahashi M, Urakawa O (2003) Biaxial damping function of entangled monodisperse polystyrene melts: comparison with the Mead-Larson-Doi model. *J Rheol* 47:1201–1210
- Lake GJ, Thomas AG (1967) The strength of highly elastic materials. *Proc R Soc Lond A* 300:108–119
- Malkin AY, Petrie C (1997) Some conditions for rupture of polymer liquids in extension. *J Rheol* 41:1–25
- Mazich KA, Samus M (1990) Role of entanglement couplings in threshold fracture of a rubber network. *Macromolecules* 23:2478–2483
- Menezes E, Graessley W (1982) Nonlinear rheological behavior of polymer systems for several shear-flow histories. *J Poly Sci Part B: Poly Phys* 20:1817–1833
- Narimissa E, Wagner MH (2019) Review on tube model based constitutive equations for polydisperse linear and long-chain branched polymer melts. *J Rheol* 63:361–375
- Narimissa E, Huang Q, Wagner MH (2020a) Elongational rheology of polystyrene melts and solutions: concentration dependence of the interchain tube pressure effect. *J Rheol* 64:95–110
- Narimissa E, Schweizer T, Wagner MH (2020b) A constitutive analysis of nonlinear shear flow. *Rheol Acta* 59:487–506
- Narimissa E, Poh L, Wagner MH (2021) Elongational viscosity scaling of polymer melts with different chemical constituents. *Rheol Acta* 60:163–174
- Osaki K, Nishizawa K, Kurata M (1982) Material time constant characterizing the nonlinear viscoelasticity of entangled polymeric systems. *Macromolecules* 15:1068–1071
- Rolon-Garrido VH, Wagner MH, Luap C, Schweizer T (2006) Modeling non-Gaussian extensibility effects in elongation of nearly monodisperse polystyrene melts. *J Rheol* 50:327–340
- Shahid T (2018). Understanding and modelling the extensional rheology of nearly monodisperse linear polymers. PhD Thesis KU Leuven, Belgium. <https://dial.uclouvain.be/pr/boreal/object/boreal:203674>
- Takahashi M, Isaki T, Takigawa T, Masuda T (1993) Measurement of biaxial and uniaxial extensional flow behavior of polymer melts at constant strain rates. *J Rheol* 37:827–846
- Wagner MH (1990) The nonlinear strain measure of polyisobutylene melt in general biaxial flow and its comparison to the Doi-Edwards model. *Rheol Acta* 29:594–603
- Wagner MH, Schaeffer J (1992) Nonlinear measures for general biaxial extension of polymer melts. *J Rheol* 36:1–26
- Wagner MH, Rubio P, Bastian H (2001) The molecular stress function model for polydisperse polymer melts with dissipative convective constraint release. *J Rheol* 45:1387–1412
- Wagner MH, Yamaguchi M, Takahashi M (2003) Quantitative assessment of strain hardening of low-density polyethylene melts by the molecular stress function model. *J Rheol* 47:779–793
- Wagner MH, Kheirandish S, Hassager O (2005) Quantitative prediction of transient and steady-state elongational viscosity of nearly monodisperse polystyrene melts. *J Rheol* 49:1317–1327
- Wagner MH (2014) Scaling relations for elongational flow of polystyrene melts and concentrated solutions of polystyrene in oligomeric styrene. *Rheol Acta* 53:765–777
- Wagner MH, Narimissa E, Huang Q (2018) On the origin of brittle fracture of entangled polymer solutions and melts. *J Rheol* 62:221–223
- Wagner MH, Narimissa E, Huang Q (2021) Scaling relations for brittle fracture of entangled polystyrene melts and solutions in elongational flow. *J Rheol* 65:311–324
- Winter HH, Mours M (2006) The cyber infrastructure initiative for rheology. *Rheol Acta* 45:331–338

**Publisher's note** Springer Nature remains neutral with regard to jurisdictional claims in published maps and institutional affiliations.